

Giant tunability of interlayer friction in graphite via ion intercalation

Zhenqian Pang^{a,1}, Jiayu Wan^{b,*}, Aijiang Lu^b, Jiaqi Dai^b, Liangbing Hu^{b,*}, Teng Li^{a,*}

^a Department of Mechanical Engineering, University of Maryland College Park, College Park, MD, 20742, United States of America

^b Department of Materials Science and Engineering, University of Maryland College Park, College Park, MD, 20742, United States of America

ARTICLE INFO

Article history:

Received 12 October 2019

Received in revised form 21 November 2019

Accepted 1 December 2019

Available online 4 December 2019

Keywords:

Friction

Ion intercalation

Graphite

Density functional theory

ABSTRACT

Two dimensional (2D) materials have attracted great interest due to their unique structures and properties. However, the loss of the exceptional properties of 2D constituents in their 3D counterparts poses a grand challenge to the widespread use of 2D materials. How to achieve comparable superior properties in 3D materials made of 2D constituents still remains elusive. Here we demonstrate an effective approach to tailoring the mechanical properties of 3D materials, made of 2D constituents via ion intercalation. We show that, by intercalating Li ions into graphite, the inter-graphene-layer friction can be drastically increased up to 7 times of that in natural graphite. We attribute the drastic increase of inter-graphene-layer friction to the electrostatic interaction of graphene layers with the intercalants. The layered structure of 2D materials and the weak inter-layer interactions allow for facile intercalation of various foreign species into the vdW gap of 2D materials. Therefore, fertile opportunities exist to leverage ion intercalation to fine tune the interlayer interaction between 2D constituents, paving a promising way to programmable mechanical properties of their 3D counterpart materials.

© 2019 Elsevier Ltd. All rights reserved.

1. Introduction

Two dimensional (2D) materials, such as graphene [1–3], molybdenum disulfide [4], hexagonal boron nitride [5] and MXenes [6,7] have received tremendous attention in the past two decades due to their atomically thin planar structures as well as their superb physical and chemical properties [8,9]. The mechanical properties of 2D materials are remarkable (e.g., graphene is the strongest material ever measured with an intrinsic strength of 130 GPa) [10], and also can be leveraged to tailor other properties of 2D materials (e.g., electromagnetic and optical) [10–16]. Enthusiasm for the significant potentials of 2D materials aside, how to achieve comparable superior properties in 3D materials made of 2D constituents still remains elusive. The loss of exceptional properties of 2D constituents in their 3D counterparts poses a grand challenge to the widespread use of 2D materials, and thus calls for an effective and general solution.

The layered structure of 2D materials and the weak inter-layer interactions allow for facile intercalation of foreign species into the vdW gap of 2D materials. Intercalation can provide the highest doping to 2D materials and enable continuous, reversible and intrinsic modifications to the host material, suggesting an effective mechanism to tune the properties of the 2D materials [17,

18]. So far, intercalation method has been successfully applied to tailor the properties of 2D materials toward optical [19–21], electrical [22–25], optoelectronic [26–28], magnetic [29,30], thermoelectric [31], energy conversion [32] and storage [33] applications. The intercalating species can cause significant charge transport in the host 2D materials, which in turn can change the mechanical properties of the 2D materials. There exist fertile opportunities to leverage intercalation to tune the mechanical properties of 2D materials, which remain largely unexplored to date.

In this letter, we reveal the giant tunability of friction in between graphene via intercalation of Li ions, epitomizing the remarkable potential of ion intercalation to tailor the mechanical properties 3D materials made of 2D constituents. Using density functional theory (DFT) calculations, we show that, by intercalating Li ions into neighboring graphene layers, the inter-graphene-layer friction can be drastically increased up to 7 times of that in natural graphite. The level of interlayer friction can be effectively programmed via controlling ion intercalation level, demonstrating facile tunability. Such a result is counterintuitive, given that intercalation species increase the distance between graphene layers, which is supposed to decrease the inter-graphene-layer interactions and thus leads to decreasing friction. We attribute the drastic increase of inter-graphene-layer friction to the electrostatic interaction of graphene layers with the intercalants. The charge transfer of the intercalants to graphene layers gives rise to the opposite electric plane of graphene and the intercalants. The resulting electrostatic attractive force between the neighboring graphene layer (-) and the Li intercalants (+) leads to

* Corresponding authors.

E-mail addresses: jiayuw@umd.edu (J. Wan), binghu@umd.edu (L. Hu), lit@umd.edu (T. Li).

¹ These authors contributed equally to this work.

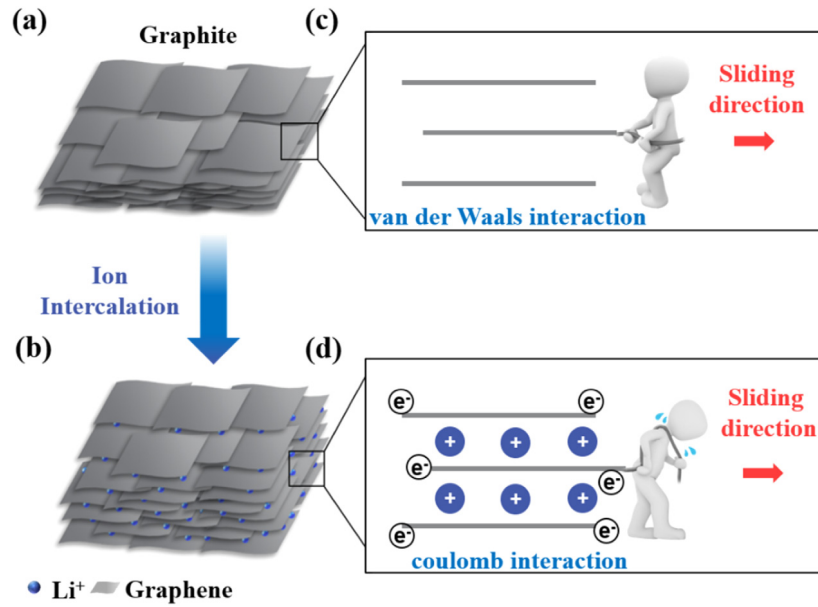


Fig. 1. Schematic of graphitic carbon before (a) and after (b) Li ion intercalations. Carbon is shown in gray and Li ions in blue. Schematic images illustrate friction force between graphene layers before (c) and after (d) Li ion intercalation. The local structure is zoomed in with 3 graphitic layers shown on the right side of the figure. The friction force increases remarkably due to Li ion intercalation induced Coulomb interaction between the graphene layers and Li ions.

the enhanced friction between the neighboring graphene layers (Fig. 1).

A variety of intercalating species (e.g., ions, metals, organic and inorganic molecules [17,31,34,35]) have been demonstrated for 2D materials, which are expected to have different effects on charge transfer in host 2D materials. Therefore, there exist promising potentials to leverage ion intercalation to fine-tune the interlayer friction between 2D constituents, paving a way toward programmable mechanical properties of their 3D counterpart materials.

2. Energy barrier and friction force during interlayer sliding

To quantitatively compare the interlayer friction of pristine graphite and that of Li-intercalated graphite, we carry out DFT calculations to simulate the interlayer sliding in these two cases (Fig. 2, see Method sections for simulation details). It is shown that at the beginning of Li intercalation process the distribution of Li ions is heterogeneous. But as the intercalation process proceeds, the lithiated area increases linearly with time and the distribution of the Li ions converges to a uniform profile eventually at equilibrium [26]. Thus, we implement all the DFT simulations based on the equilibrium state of Li-intercalated graphite system and assume a uniform distribution of Li ions. Pristine graphene layers prefer AB stacking, while intercalated ions shift the stacking pattern of graphite to AA stacking [36]. It has also been confirmed that the center of the hexagon ring is the most favored intercalation site with the maximum absorption energy [37,38].

Fig. 2a shows the perspective views of the simulation models of pristine graphite (left) and ion-intercalated graphite (right), respectively. The arrows illustrate the two representative sliding directions of the middle graphene layer, namely, armchair direction (AC) and zigzag direction (ZZ). Fig. 2b shows four repeating steps in the sliding process along AC direction for pristine graphite (left, labeled as $P_0^{AC} \sim P_3^{AC}$) and ion intercalated graphite (right, labeled as $Q_0^{AC} \sim Q_3^{AC}$), respectively. Fig. 2c shows two repeating steps in the sliding process along ZZ direction for pristine graphite (left, labeled as $P_0^{ZZ} \sim P_1^{ZZ}$) and ion intercalated graphite (right, labeled as $Q_0^{ZZ} \sim Q_1^{ZZ}$), respectively. P_0 and Q_0 positions

correspond to the thermodynamically stable structures with the lowest energy.

Fig. 2d plots the variation of energy per atom from the lowest energy states (i.e., P_0 or Q_0) as the function of sliding displacement, D , in AC direction, for pristine graphite (blue) and ion-intercalated graphite (red), respectively. Here for comparison, we consider the case of maximum intercalation capacity for the Li/graphite system [39] (with a ratio of Li:C=1:6). For pristine graphite, the highest energy variation (defined as the energy barrier of sliding process) is 0.011 eV/atom, occurring at the sliding displacement of 2.7 Å, which corresponds to P_3^{AC} position (Fig. 2b, AA stacking). For ion-intercalated graphite, the graphene interlayer distance increases from 3.4 Å to 3.7 Å (about 10%), consistent with the experimental results [40]. The energy variation as the function of sliding displacement shows a symmetric double-peak shape, with an energy barrier of 0.079 eV/atom, more than 7 times of that of pristine graphite. The two energy barriers occur at the sliding displacements of 1.43 Å and 2.86 Å, corresponding to Q_1^{AC} and Q_3^{AC} , respectively. There exists a local minimum of energy variation (Q_2^{AC} , 0.069 eV/atom) between these two energy barriers, corresponding to the sliding position when the Li ion is above the center of the C-C bond in the middle graphene layer.

Fig. 2e plots the variation of energy per atom from the lowest energy states (i.e., P_0 or Q_0) as the function of sliding displacement, D , in ZZ direction, for pristine graphite (blue) and ion-intercalated graphite (red), respectively. Different from sliding along AC direction, there exists only one peak of energy variation (i.e., energy barrier) when sliding along ZZ direction. For example, the energy barrier for pristine graphite sliding is 0.009 eV/atom (occurring at P_1^{ZZ} position), while the energy barrier for ion-intercalated graphite sliding is 0.069 eV/atom (occurring at Q_1^{ZZ} position), a more than 7-time increase. Note that the energy barrier along ZZ sliding direction is the same as the local minimum of energy variation along AC sliding direction (0.069 eV/atom), due to the same atomic structure (i.e., Q_1^{ZZ} is identical to Q_2^{AC}).

Figs. 2f and 2g plot the friction force (calculated by taking the derivative of the curves in Fig. 2d) as the function of sliding displacement, D , in AC and ZZ directions, respectively (pristine graphite: blue and ion-intercalated graphite: red). The friction force in ion-intercalated graphite (0.085 eV/Å/atom) is 7 times

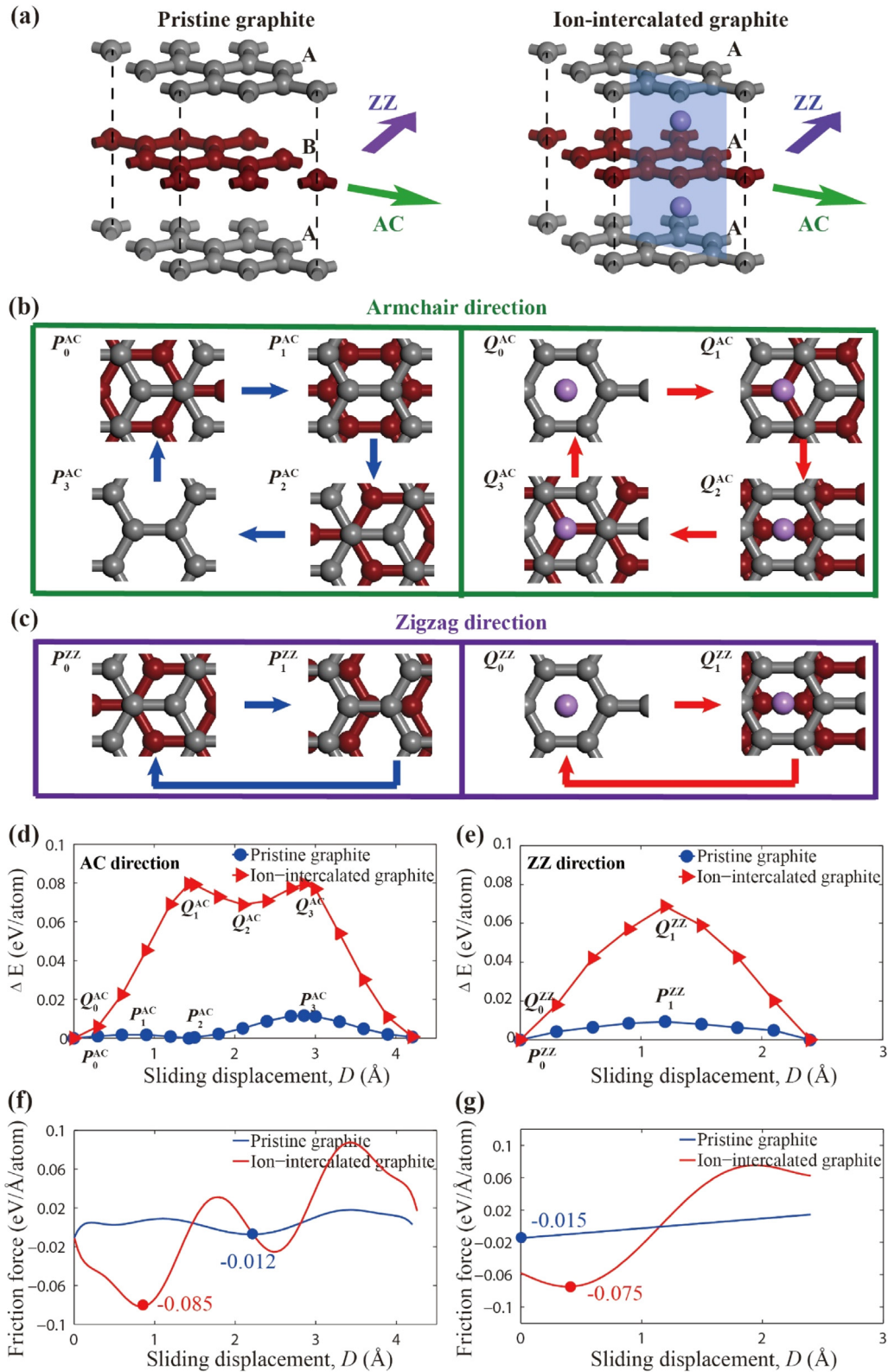


Fig. 2. Derivation of energy and friction before and after Li intercalation. (a) Perspective views of the simulation models of pristine graphite (left) and ion-intercalated graphite (right). The shade in the right panel illustrates the cross-section for which the charge density is computed in Fig. 3. (b) Atomic structures in the sliding process along AC direction for pristine graphite (left, labeled as $P_0^{AC} \sim P_3^{AC}$) and ion intercalated graphite (right, labeled as $Q_0^{AC} \sim Q_3^{AC}$). (c) Atomic structures in the sliding process along ZZ direction for pristine graphite (left, labeled as $P_0^{ZZ} \sim P_1^{ZZ}$) and ion intercalated graphite (right, labeled as $Q_0^{ZZ} \sim Q_1^{ZZ}$). (d) Variation of energy per atom as the function of sliding displacement, D , in AC (d) and ZZ direction (e). Corresponding friction force as the function of sliding displacement, D , in AC (f) and ZZ (g) directions.

higher than that in pristine graphite (0.012 eV/Å/atom) when sliding along AC direction, and 5 times higher when sliding along ZZ direction (0.075 eV/Å/atom vs. 0.015 eV/Å/atom).

For the sliding of large-scale graphene flakes, the shear lag effect should be considered. A shear-lag model [41,42] predicts the critical sliding strain ε_c in the graphene layer as

$$\varepsilon_c = -\sqrt{\frac{\Delta E}{E_g t_g}} \coth(\beta L) \quad (1)$$

where ΔE is the variation of interfacial energy after sliding and L is the original length of the large scale graphene in its in-plane direction. $\beta = \sqrt{\frac{K_g}{E_g t_g}}$ is the shear lag parameter, where K_g is the interface stiffness, E_g is Young's modulus and t_g is the thickness of graphene.

When the applied strain reaches the ε_c , the sliding occurs at the edge of the graphene. As the applied strain furthers increases, the sliding zones increase. When the whole graphene flake slides, the maximum stress (τ_{max}) and strain (ε_{max}) can be given by

$$\tau_{max} = -\sqrt{2\Delta E K_g} \quad (2)$$

$$\varepsilon_{max} = -\frac{\sqrt{2\Delta E K_g} L}{E_g t_g} \quad (3)$$

Our DFT calculation reveals a significant increase in interfacial energy after Li intercalation (more than 7 times increase, Fig. 2(d) and (e)). Such a large variation of interfacial energy leads to an increased critical strain of initial sliding (from Eq. (1)) and an increased level of maximum stress and strain to slide the whole graphene (from Eqs. (2) and (3)). Given the square root dependence of τ_{max} on ΔE , the friction force due to interlayer sliding in ion-intercalated graphite can still be 2.65 times higher than that in pristine graphite, by considering the shear-lag effect.

3. Charge density and projected density of states

To offer mechanistic understanding of the drastic increase of interlayer friction in ion-intercalated graphite, we consider the influence of ion intercalation on the electronic behavior of graphite. Previous studies reveal that, upon Li intercalation, carbon atoms in a carbon nanotube can be negatively charged with electrons transferred from Li [43]. Through Mulliken Population analysis, we show that the intercalated Li ions are able to transfer as much as 0.89 electron charge per Li ion to the graphene plane, which is consistent with other reports [44]. Thus, we attribute the drastic increase of interlayer friction in ion-intercalated graphite to the Coulombic attraction between the graphene layers and Li ion layers.

To further elaborate the Li ion induced electron transfer to graphene layers, we calculate the evolution of charge densities in the Li ion intercalated graphite during the sliding process along AC direction, as shown in Fig. 3a. Here, we consider the sliding process in two representative stages: energy increasing stage (from Q_0^{AC} to Q_1^{AC} : $D = 0 \sim 1.43$ Å) and energy decreasing stage (from Q_1^{AC} to Q_2^{AC} : $D = 1.43$ Å \sim 2.1 Å). As shown in the first panel of Fig. 3 ($D = 0$ Å), the Li intercalants lead to electron transfer to both sides of each graphene layer in the graphite. This is distinct from pristine graphite where the interlayer interaction is essentially van der Waals type and there is no electron transfer.

In the energy increasing stage ($D = 0 \sim 1.43$ Å), the distribution of charge density in the sliding graphene layer becomes more non-uniform as the sliding proceeds. The charge density on the carbon atom reaches the highest when it passes right beneath the Li intercalant (i.e., Q_1^{AC} position). Such an increasing non-uniformity of charge density corresponds to the increase of energy as shown in Fig. 2d. In the energy decreasing stage

($D = 1.43 \sim 2.1$ Å), the distribution of charge density in the sliding graphene layer tends to be more uniform as the sliding proceeds. When the Li intercalant reaches the middle of the C-C bond (i.e., Q_2^{AC} position), the charge density on the two carbon atoms becomes identical. Such an increasing uniformity of charge density corresponds to the decrease of energy as shown in Fig. 2d.

Furthermore, to investigate the distribution of orbital electron to the charge transfer, the projected density of states (PDOS) of the whole system is calculated at different graphene sliding steps (from $Q_0^{AC}Q_0^{AC}$ to Q_2^{AC}) after Li intercalation, as shown in Fig. 4a. There exists a distinct difference of PDOS (contributed by p orbital, blue curves) near the Fermi level at different sliding steps. In the energy increasing stage, PDOS near the Fermi level increases significantly from 1.41 at Q_0^{AC} position to 2.51 at Q_1^{AC} position, while in the energy decreasing stage, PDOS near the Fermi level decreases gradually from 2.51 at Q_1^{AC} position to 2.00 at Q_2^{AC} position. The more occupied states near the Fermi level correspond to higher electronic energy and better electron-donating capability. Therefore, the capability of electron donating from Li intercalant to the graphitic matrix reaches the maximum at Q_1^{AC} position, corresponding to the strongest Coulombic interaction. The above variation of PDOS near the Fermi level is consistent with the variations of energy (Fig. 2d) and charge density (Fig. 3) during the sliding process. It can be concluded that the p -electron near the Fermi level dominates the variation of energy, thus forms the energy barrier of the interlayer sliding of graphite. To evaluate the contribution of different atoms, the PDOS of Li and C atoms are calculated simultaneously (Fig. 4b). It is shown that the C atoms make a dominating contribution to the p -electron, while the influence from Li atoms is negligible.

4. Tunability of interlayer friction

The interlayer friction of graphite can be further fine tuned by tailoring the Li intercalation level in graphite. For example, by controlling the state of charge of a graphite/Li half cell, the Li intercalation level can be quantitatively programmed. Fig. 5a illustrates the electrochemical Li intercalation staging effect in graphite, obtained by charging/discharging a graphite/Li half cell with liquid electrolyte (1M LiPF₆: Ethylene Carbonate: Diethyl Carbonate) at a charging rate of C/20.

From the voltage profiles shown in Fig. 5a, three intercalation levels (such as LiC₃₆, Li₃C₃₆ and Li₆C₃₆, respectively) can be achieved during both Li intercalation (blue curve) and deintercalation (red curve) in graphite. The highly reversible staging effect of Li intercalation in graphite indicates the promising potential of using electrochemical method as an effective approach to programming the interlayer friction of graphite. Fig. 5b shows the programmable friction force in graphite as a function of Li intercalation level in graphite. As the Li intercalation level increases, the interlayer friction in graphite increases.

5. Concluding remark

In summary, we reveal an effective approach to tailoring the interlayer friction of graphite by ion intercalation. We demonstrate that using Li intercalation, the interlayer friction of graphite can be substantially increased up to 7 times. We further show that the interlayer friction of graphite can be programmed by controlling the level of Li intercalation.

Our DFT calculations reveal that the enhanced interlayer friction of graphite via Li intercalation results from the increased Coulombic interaction between the graphene layers and the intercalants. By contrast, the interaction between graphene layers in pristine graphite is largely van der Waals type. Further analysis

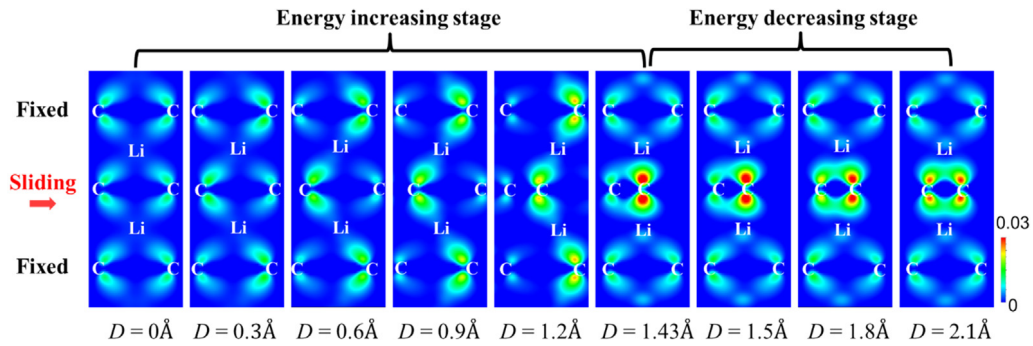


Fig. 3. Cross-sectional views of charge density during the sliding process along AC direction. Cross section is shown as shadow area in Fig. 2a. The middle graphene layer slides and the top and bottom graphene layers are fixed. Red arrow represents the sliding direction. (Unit of the color scale: e/Bohr^3 .)

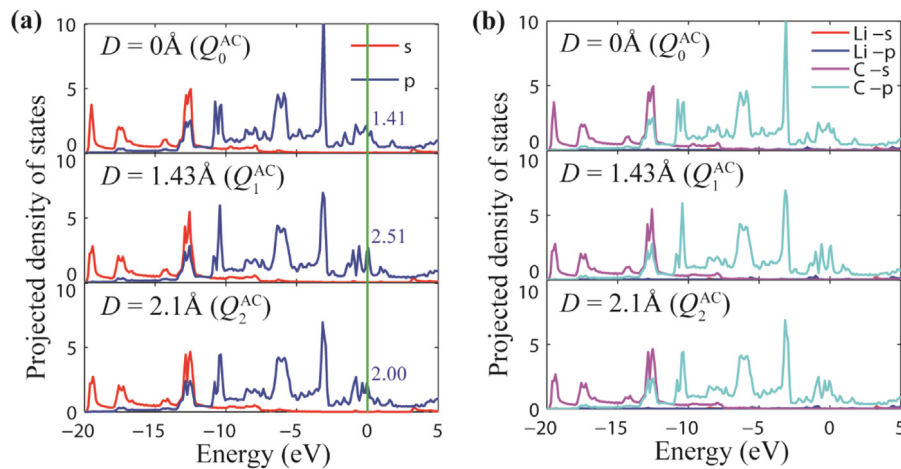


Fig. 4. The projected density of states (PDOS) changes in the sliding process along AC direction: (a) total and (b) partial.

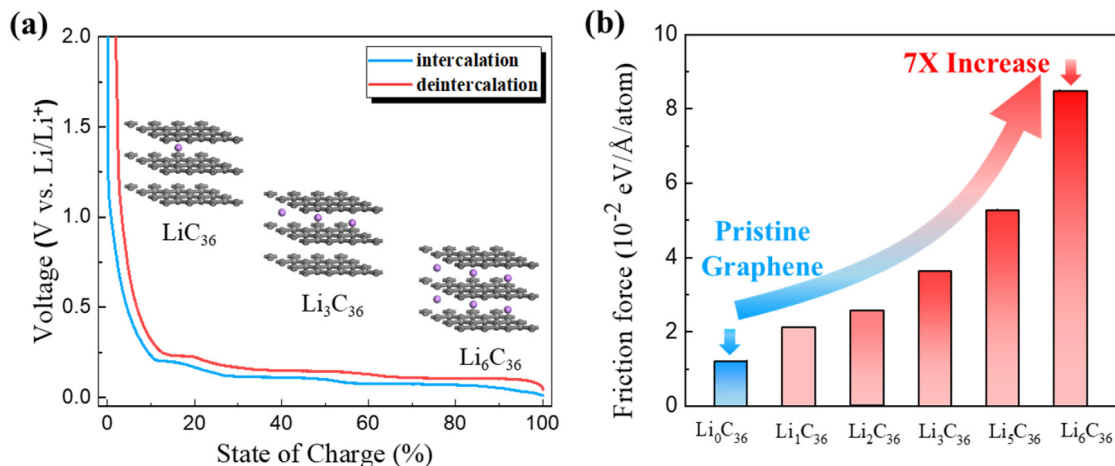


Fig. 5. Programmable interlayer friction of graphite. (a) voltage profile of Li intercalation in graphite with a Li/graphite half cell (electrolyte of 1M LiPF₆ in EC/DEC v:v=1:1) (b) interlayer friction of graphite with different Li intercalation level.

shows that there exist two stages in the interlayer sliding process of ion-intercalated graphite, giving rise to distinctive charge transfer behaviors. In the energy increasing stage, the distribution of charge density in the sliding graphene layer becomes more non-uniform, while the charge density becomes more uniform in the energy decreasing stage. PDOS calculation shows that p -electron near the Fermi level dominates the variation of energy and forms the energy barrier of the interlayer sliding of graphite.

Research findings from the present work shed light on tuning the charge transfer in other 2D materials and van der Waals

heterostructures, which in turn provide a fertile ground for programmable mechanical properties of 3D materials made of 2D building blocks.

Methods

Density functional theory (DFT) implemented in the Vienna ab initio simulation package (VASP) [45,46] is performed to determine the atomic interaction between Li and graphene. The

generalized gradient approximation (GGA) of the Perdew–Burke–Ernzerhof (PBE) [47] functional is used for exchange and correlation interaction. We have tested the validity of PBE calculations by examining its predictability for the lattice constant of graphene [37]. The result from PBE calculation is in good agreement with the experiments [48]. Considering the symmetry of graphene with maximum Li insertion, A $\sqrt{3} \times \sqrt{3}$ rhombus supercell is used to investigate the interaction of Li atoms with pristine graphene. In order to compare with the results stretching graphene layer without Li insertion, the VDW correction, which is described by DFT-D2 method of Grimme [49], is considered in all these calculations. The Brillouin zone is sampled by a $6 \times 6 \times 4$ Monkhorst and Pack [50] grid. The cutoff energy in our calculation is 500 eV. All the calculations are relaxed to minimize the total energy of the system until the atomic forces are converged to 0.01 eV/Å. Periodical boundary conditions are applied in both in-plane and interlayer directions. The assumption of uniform distribution of Li ions and the periodic boundary condition of our simulation model, in combination with the large bending stiffness of the graphene layer [51] result in the relatively uniform increase of interlayer distance of graphene after Li intercalation. In reality, the non-uniform distribution of Li ions could result in fluctuation of graphene morphology, for example, having a smaller interlayer distance in domains without Li ions and a larger interlayer distance in domains with concentrated Li ions. Such a fluctuating morphology of graphene is expected to modestly increase the interlayer friction [52,53], as it takes additional energy to accommodate the variation of graphene morphology as the interlayer sliding occurs. As we focus on the friction between the graphene layers, the upper and lower graphene layers are fixed in their plane and the middle graphene layer slides along AC or ZZ direction. The Li intercalants are free along the sliding direction and then the structures are relaxed sufficiently.

Here we define the variation of energy per atom as $\Delta E = (E_{total} - E_{origin})/n$, where E_{total} is the total energy of the Li intercalated graphene layer and E_{origin} is the energy of the system before the sliding process, and n is the total number of carbon atoms. The maximum value of ΔE is defined as the energy barrier of the sliding process.

The friction force is computed by taking the derivative of the energy curve $\vec{F} = \nabla E$. The maximum of the frictional force characterizes the threshold resistance to overcome during sliding.

Declaration of competing interest

The authors declare that they have no known competing financial interests or personal relationships that could have appeared to influence the work reported in this paper.

CRediT authorship contribution statement

Zhenqian Pang: Data curation, Writing - Original draft, Writing - reviewing & editing. **Jiayu Wan:** Data curation, Writing - original draft. **Aijiang Lu:** Data curation, Writing - original draft. **Liangbing Hu:** Conceptualization, Methodology, Supervision. **Teng Li:** Conceptualization, Methodology, Supervision, Writing - reviewing & editing.

Acknowledgments

Z. Pang and T. Li acknowledge the University of Maryland supercomputing resources (<http://hpc.umd.edu>) made available for conducting the research reported in this paper. T. Li acknowledges the support by the National Science Foundation, United States of America (Grant # CMMI-1129826). L. Hu acknowledges the support from the National Science Foundation, United States of America (Grant # CBET-1335979).

References

- [1] A.K. Geim, K.S. Novoselov, The rise of graphene, *Nature Mater.* 6 (2007) 183–191, <http://dx.doi.org/10.1038/nmat1849>.
- [2] X. Yang, C. Cheng, Y. Wang, L. Qiu, D. Li, Liquid-mediated dense integration of graphene materials for compact capacitive energy storage, *Science* 341 (2013) 534 LP -537, URL <http://science.sciencemag.org/content/341/6145/534abstract>.
- [3] A.K. Geim, Graphene: Status and prospects, *Science* 324 (2009) 1530–1534, <http://dx.doi.org/10.1126/science.1158877>.
- [4] K.F. Mak, C. Lee, J. Hone, J. Shan, T.F. Heinz, Atomically thin MoS₂: A new direct-gap semiconductor, *Phys. Rev. Lett.* 105 (2010) 136805, <http://dx.doi.org/10.1103/PhysRevLett.105.136805>.
- [5] C. Jin, F. Lin, K. Suenaga, S. Iijima, Fabrication of a freestanding boron nitride single layer and its defect assignments, *Phys. Rev. Lett.* 102 (2009) 195505, <http://dx.doi.org/10.1103/PhysRevLett.102.195505>.
- [6] F. Shahzad, M. Alhabeab, C.B. Hatter, B. Anasori, S.M. Hong, C.M. Koo, Y. Gogotsi, Electromagnetic interference shielding with 2d transition metal carbides (MXenes), *Science* (2016) <http://dx.doi.org/10.1126/science.aag2421>.
- [7] M.R. Lukatskaya, O. Mashtalir, C.E. Ren, Y. Dall'Agnese, P. Rozier, P.L. Taberna, M. Naguib, P. Simon, M.W. Barsoum, Y. Gogotsi, Cation intercalation and high volumetric capacitance of two-dimensional titanium carbide, *Science* (2013) <http://dx.doi.org/10.1126/science.1241488>.
- [8] S.Z. Butler, S.M. Hollen, L. Cao, Y. Cui, J.A. Gupta, H.R. Gutiérrez, T.F. Heinz, S.S. Hong, J. Huang, A.F. Ismach, E. Johnston-Halperin, M. Kuno, V.V. Plashnitsa, R.D. Robinson, R.S. Ruoff, S. Salahuddin, J. Shan, L. Shi, M.G. Spencer, M. Terrones, W. Windl, J.E. Goldberger, Progress, challenges, and opportunities in two-dimensional materials beyond graphene, *ACS Nano* 7 (2013) 2898–2926, <http://dx.doi.org/10.1021/nn400280c>.
- [9] M. Chhowalla, H.S. Shin, G. Eda, L.-J. Li, K.P. Loh, H. Zhang, The chemistry of two-dimensional layered transition metal dichalcogenide nanosheets, *Nature Chem.* 5 (2013) 263–275, <http://dx.doi.org/10.1038/nchem.1589>.
- [10] C. Lee, X. Wei, J.W. Kysar, J. Hone, Measurement of the elastic properties and intrinsic strength of monolayer graphene, *Science* 321 (2008) 385–388, <http://dx.doi.org/10.1126/science.1157996>.
- [11] G.-H. Lee, R.C. Cooper, S.J. An, S. Lee, A. van der Zande, N. Petrone, A.G. Hammerberg, C. Lee, B. Crawford, W. Oliver, J.W. Kysar, J. Hone, High-strength chemical-vapor-deposited graphene and grain boundaries, *Science* 340 (2013) 1073–1076, <http://dx.doi.org/10.1126/science.1235126>.
- [12] S. Zhu, J.A. Stroschio, T. Li, Programmable extreme pseudomagnetic fields in graphene by a uniaxial stretch, *Phys. Rev. Lett.* 115 (2015) <http://dx.doi.org/10.1103/PhysRevLett.115.245501>.
- [13] D. Akinwande, C.J. Brennan, J.S. Bunch, P. Egberts, J.R. Felts, H. Gao, R. Huang, J.S. Kim, T. Li, Y. Li, K.M. Liechti, N. Lu, H.S. Park, E.J. Reed, P. Wang, B.I. Yakobson, T. Zhang, Y.W. Zhang, Y. Zhou, Y. Zhu, A review on mechanics and mechanical properties of 2d materials—Graphene and beyond, *Extrem. Mech. Lett.* 13 (2017) 42–77, <http://dx.doi.org/10.1016/j.eml.2017.01.008>.
- [14] P. Zhang, L. Ma, F. Fan, Z. Zeng, C. Peng, P.E. Loya, Z. Liu, Y. Gong, J. Zhang, X. Zhang, P.M. Ajayan, T. Zhu, J. Lou, Fracture toughness of graphene, *Nature Commun.* 5 (2014) <http://dx.doi.org/10.1038/ncomms4782>.
- [15] N. Levy, S.A. Burke, K.L. Meaker, M. Panlasigui, A. Zettl, F. Guinea, A.H.C. Neto, M.F. Crommie, Strain-induced pseudo-magnetic fields greater than 300 t in graphene nanobubbles, *Science* 329 (2010) 544–547, <http://dx.doi.org/10.1126/science.1191700>.
- [16] N.N. Klimov, S. Jung, S. Zhu, T. Li, C.A. Wright, S.D. Solares, D.B. Newell, N.B. Zhitenev, J.A. Stroschio, Electromechanical properties of graphene drumheads, *Science* 336 (2012) 1557–1561, <http://dx.doi.org/10.1126/science.1220335>.
- [17] J. Wan, S.D. Lacey, J. Dai, W. Bao, M.S. Fuhrer, L. Hu, Tuning two-dimensional nanomaterials by intercalation: materials, properties and applications, *Chem. Soc. Rev.* 45 (2016) 6742–6765, <http://dx.doi.org/10.1039/C5CS00758E>.
- [18] Y. Jung, Y. Zhou, J.J. Cha, Intercalation in two-dimensional transition metal chalcogenides, *Inorg. Chem. Front.* 3 (2016) 452–463, <http://dx.doi.org/10.1039/C5QI00242G>.
- [19] J.J. Cha, K.J. Koski, K.C.Y. Huang, K.X. Wang, W. Luo, D. Kong, Z. Yu, S. Fan, M.L. Brongersma, Y. Cui, Two-dimensional chalcogenide nanoplates as tunable metamaterials via chemical intercalation, *Nano Lett.* 13 (2013) 5913–5918, <http://dx.doi.org/10.1021/nl402937g>.
- [20] K.P. Chen, F.R. Chung, M. Wang, K.J. Koski, Dual element intercalation into 2D layered Bi₂Se₃ nanoribbons, *J. Am. Chem. Soc.* 137 (2015) 5431–5437, <http://dx.doi.org/10.1021/jacs.5b00666>.
- [21] M. Wang, K.J. Koski, Reversible chemochromic moo₃ nanoribbons through zerovalent metal intercalation, *ACS Nano* 9 (2015) 3226–3233, <http://dx.doi.org/10.1021/acsnano.5b00336>.
- [22] Y. Yu, F. Yang, X.F. Lu, Y.J. Yan, Y.-H. Cho, L. Ma, X. Niu, S. Kim, Y.-W. Son, D. Feng, S. Li, S.-W. Cheong, X.H. Chen, Y. Zhang, Gate-tunable phase transitions in thin flakes of 1T-TaS₂, *Nature Nanotechnology* 10 (2015) 270–276, <http://dx.doi.org/10.1038/nnano.2014.323>.

- [23] Z. Zeng, Z. Yin, X. Huang, H. Li, Q. He, G. Lu, F. Boey, H. Zhang, Single-layer semiconducting nanosheets: High-yield preparation and device fabrication, *Angew. Chem., Int. Ed. Engl.* 50 (2011) 11093–11097, <http://dx.doi.org/10.1002/anie.201106004>.
- [24] C. Wang, Q. He, U. Halim, Y. Liu, E. Zhu, Z. Lin, H. Xiao, X. Duan, Z. Feng, R. Cheng, N.O. Weiss, G. Ye, Y.C. Huang, H. Wu, H.C. Cheng, I. Shakir, L. Liao, X. Chen, W.A. Goddard, Y. Huang, X. Duan, Monolayer atomic crystal molecular superlattices, *Nature* 555 (2018) 231–236, <http://dx.doi.org/10.1038/nature25774>.
- [25] D.K. Bediako, M. Rezaee, H. Yoo, D.T. Larson, S.Y.F. Zhao, T. Taniguchi, K. Watanabe, T.L. Brower-Thomas, E. Kaxiras, P. Kim, Heterointerface effects in the electrointercalation of van der Waals heterostructures, *Nature* 558 (2018) 425–429, <http://dx.doi.org/10.1038/s41586-018-0205-0>.
- [26] W. Bao, J. Wan, X. Han, X. Cai, H. Zhu, D. Kim, D. Ma, Y. Xu, J.N. Munday, H.D. Drew, M.S. Fuhrer, L. Hu, Approaching the limits of transparency and conductivity in graphitic materials through lithium intercalation, *Nature Commun.* 5 (2014) <http://dx.doi.org/10.1038/ncomms5224>.
- [27] J. Wan, F. Gu, W. Bao, J. Dai, F. Shen, W. Luo, X. Han, D. Urban, L. Hu, Sodium-ion intercalated transparent conductors with printed reduced graphene oxide networks, *Nano Lett.* 15 (2015) 3763–3769, <http://dx.doi.org/10.1021/acs.nanolett.5b00300>.
- [28] J. Yao, K.J. Koski, W. Luo, J.J. Cha, L. Hu, D. Kong, V.K. Narasimhan, K. Huo, Y. Cui, Optical transmission enhancement through chemically tuned two-dimensional bismuth chalcogenide nanoplates, *Nature Commun.* 5 (2014) 5670, <http://dx.doi.org/10.1038/ncomms6670>.
- [29] W.J. Hardy, C.W. Chen, A. Marcinkova, H. Ji, J. Sinova, D. Natelson, E. Morosan, Very large magnetoresistance in Fe_{0.28}TaS₂ single crystals, *Phys. Rev. B* 91 (2015) <http://dx.doi.org/10.1103/PhysRevB.91.054426>.
- [30] E. Morosan, H.W. Zandbergen, L. Li, M. Lee, J.G. Checkelsky, M. Heinrich, T. Siegrist, N.P. Ong, R.J. Cava, Sharp switching of the magnetization in Fe_{1/4}TaS₂, *Phys. Rev. B* 75 (2007) 3–9, <http://dx.doi.org/10.1103/PhysRevB.75.104401>.
- [31] C. Wan, X. Gu, F. Dang, T. Itoh, Y. Wang, H. Sasaki, M. Kondo, K. Koga, K. Yabuki, G.J. Snyder, R. Yang, K. Koumoto, Flexible n-type thermoelectric materials by organic intercalation of layered transition metal dichalcogenide TiS₂, *Nature Mater.* 14 (2015) 622–627, <http://dx.doi.org/10.1038/nmat4251>.
- [32] H. Wang, Z. Lu, S. Xu, D. Kong, J.J. Cha, G. Zheng, P.-C. Hsu, K. Yan, D. Bradshaw, F.B. Prinz, Y. Cui, Electrochemical tuning of vertically aligned MoS₂ nanofilms and its application in improving hydrogen evolution reaction, *Proc. Natl. Acad. Sci.* 110 (2013) 19701–19706, <http://dx.doi.org/10.1073/pnas.1316792110>.
- [33] J. Wan, W. Bao, Y. Liu, J. Dai, F. Shen, L. Zhou, X. Cai, D. Urban, Y. Li, K. Jungjohann, M.S. Fuhrer, L. Hu, In situ investigations of Li-MoS₂ with planar batteries, *Adv. Energy Mater.* 1401742 (2014) 1–7, <http://dx.doi.org/10.1002/aenm.201401742>.
- [34] J. Zhang, J. Sun, Y. Li, F. Shi, Y. Cui, Electrochemical control of copper intercalation into nanoscale Bi₂Se₃, *Nano Lett.* 17 (2017) 1741–1747, <http://dx.doi.org/10.1021/acs.nanolett.6b05062>.
- [35] Y. Liu, B.V. Merinov, W.A. Goddard, Origin of low sodium capacity in graphite and generally weak substrate binding of Na and Mg among alkali and alkaline earth metals, *Proc. Natl. Acad. Sci.* 113 (2016) 3735–3739, <http://dx.doi.org/10.1073/pnas.1602473113>.
- [36] Y. Imai, A. Watanabe, Energetic evaluation of possible stacking structures of Li-intercalation in graphite using a first-principle pseudopotential calculation, *J. Alloys Compd.* (2007) <http://dx.doi.org/10.1016/j.jallcom.2006.08.061>.
- [37] Z. Pang, X. Shi, Y. Weia, D. Fang, Grain boundary and curvature enhanced lithium adsorption on carbon, *Carbon* 107 (2016) 557–563, <http://dx.doi.org/10.1016/j.carbon.2016.06.035>.
- [38] J. Zheng, Z. Ren, P. Guo, L. Fang, J. Fan, Diffusion of Li⁺ ion on graphene: A DFT study, *Appl. Surf. Sci.* 258 (2011) 1651–1655, <http://dx.doi.org/10.1016/j.apsusc.2011.09.007>.
- [39] T. Ohzuku, Formation of lithium-graphite intercalation compounds in nonaqueous electrolytes and their application as a negative electrode for a lithium ion (shuttlecock) cell, *J. Electrochem. Soc.* 140 (1993) 2490, <http://dx.doi.org/10.1149/1.2220849>.
- [40] J.R. Dahn, R. Fong, M.J. Spoon, Suppression of staging in lithium-intercalated carbon by disorder in the host, *Phys. Rev. B* 42 (1990) 6424–6432, <http://dx.doi.org/10.1103/PhysRevB.42.6424>.
- [41] T. Jiang, R. Huang, Y. Zhu, Interfacial sliding and buckling of monolayer graphene on a stretchable substrate, *Adv. Funct. Mater.* 24 (2014) 396–402, <http://dx.doi.org/10.1002/adfm.201301999>.
- [42] Z. Cui, J.-G. Guo, Theoretical investigations of the interfacial sliding and buckling of graphene on a flexible substrate, *AIP Adv.* 6 (2016) 125110, <http://dx.doi.org/10.1063/1.4973305>.
- [43] A. Udomvech, T. Kerdcharoen, T. Osotchan, First principles study of Li and Li⁺ adsorbed on carbon nanotube: Variation of tubule diameter and length, *Chem. Phys. Lett.* 406 (2005) 161–166, <http://dx.doi.org/10.1016/j.cplett.2005.02.084>.
- [44] F. Valencia, A.H. Romero, F. Ancilotto, P.L. Silvestrelli, Lithium adsorption on graphite from density functional theory calculations, *J. Phys. Chem. B* 110 (2006) 14832–14841, <http://dx.doi.org/10.1021/jp062126+>.
- [45] G. Kresse, J. Furthmüller, Efficient iterative schemes for ab initio total-energy calculations using a plane-wave basis set, *Phys. Rev. B* 54 (1996) 11169, <http://dx.doi.org/10.1103/PhysRevB.54.11169>.
- [46] G. Kresse, J. Hafner, Ab initio molecular dynamics for liquid metals, *Phys. Rev. B* 47 (1993) 558, <http://dx.doi.org/10.1103/PhysRevB.47.558>.
- [47] J. Perdew, K. Burke, M. Ernzerhof, Generalized gradient approximation made simple, *Phys. Rev. Lett.* 77 (1996) 3865–3868, <http://dx.doi.org/10.1103/PhysRevLett.77.3865>.
- [48] A.T. N'Diaye, J. Coraux, T.N. Plasa, C. Busse, T. Michely, Structure of epitaxial graphene on Ir(111), *New J. Phys.* 10 (2008) 043033, <http://dx.doi.org/10.1088/1367-2630/10/4/043033>.
- [49] S. Grimme, Semiempirical GGA-type density functional constructed with a long-range dispersion correction, *J. Comput. Chem.* 27 (2006) 1787–1799, <http://dx.doi.org/10.1002/jcc.20495>.
- [50] H.J. Monkhorst, J.D. Pack, Special points for Brillouin-zone integrations, *Phys. Rev. B* 13 (1976) 5188–5192, <http://dx.doi.org/10.1103/PhysRevB.13.5188>.
- [51] Y. Wei, B. Wang, J. Wu, R. Yang, M.L. Dunn, Bending rigidity and Gaussian bending stiffness of single-layered graphene, *Nano Lett.* 13 (2012) 26–30, <http://dx.doi.org/10.1021/nl303168w>.
- [52] T. Li, Extrinsic morphology of graphene, *Modelling Simul. Mater. Sci. Eng.* 19 (5) (2011) 054005, <http://dx.doi.org/10.1088/0965-0393/19/5/054005>.
- [53] Z. Zhang, T. Li, Determining graphene adhesion via substrate-regulated morphology of graphene, *J. Appl. Phys.* 1110 (2011) 083526, <http://dx.doi.org/10.1063/1.3656720>.